

# APPLICATION OF ADVANCED REYNOLDS STRESS TRANSPORT MODELS TO HIGHLY SEPARATED FLOWS

F. Billard, T. Craft and A. Revell

School of Mechanical, Aerospace and Civil Engineering,  
The University of Manchester, Manchester, M13 9PL, UK  
flavien.billard@manchester.ac.uk

## ABSTRACT

This paper considers the application of four Reynolds Averaged Navier Stokes (RANS) models to a range of progressively complex test cases, exhibiting both 2-D and 3-D flow separation. Two Eddy Viscosity Models (EVM) and two Reynolds Stress Transport Models (RSM) are employed, of which two (one in each category) are based on elliptic blending formulations. This study attempts to gain more insight into the importance of two modelling features for these flows; the usage of turbulence anisotropy resolving schemes and the near-wall limiting behaviour. As expected, there is no single best model, though some clear trend in performance is observed.

## INTRODUCTION

The dramatic increase in available computational power in recent years has tended to draw turbulence research away from advanced Reynolds-Averaged Navier Stokes (RANS) closures, to focus instead on approaches that fully, or partially, resolve the turbulent structures. Since fully resolved approaches (Direct Numerical Simulation) remain impractical for industrially relevant cases, a series of progressively more significant approximations are usually adopted for such applications. While Large Eddy Simulation (LES) has been successfully applied to complex flows for moderately high Reynolds numbers, the formal application of this methodology also remains computationally prohibitive for the majority of industrial flows. In particular, the sufficient resolution of near-wall structures with LES requires extremely fine meshes.

In response to the above limitations, a number of so called hybrid RANS-LES schemes have been developed across the community (see, for example Haase *et al.*, 2009; Fröhlich & von Terzi, 2008) in which the near-wall turbulence is modelled using a RANS approach, and LES employed for the outer flow regions. However, the majority of these hybrid methods retain rather simple (often linear) eddy-viscosity-based RANS closures. These simple modelling schemes are known to perform poorly in flows with, amongst other features, complex separation, reattachment, impingement, and curvature (Haase *et al.*, 2006). As such, it is relevant to question the impact of the RANS model on the hybrid solution, and the potential improvements one might gain by using a more complex scheme within such approaches.

This paper therefore attempts to explore the performance

of a number of advanced eddy-viscosity and Reynolds stress transport models in a range of flows involving challenging separation and reattachment features. The focus is on the use of such schemes within a purely RANS solution strategy, to illustrate their performance, although this will also allow some conclusions to be drawn regarding the expected performance if they were applied within the more computationally expensive hybrid approaches. A number of common 2-D flows are first examined, before two flows with 3-D effects are computed.

## DESCRIPTION OF THE MODELS

Four models are compared in the present study, namely the  $k-\omega$  SST of Menter (1994), the *SST* model of Speziale *et al.* (1991), the blended  $k-\epsilon-\bar{v}^2/k$  (BL- $\bar{v}^2/k$ ) model of Billard & Laurence (2011) and the Elliptic Blending RSM (EBRSM) of Manceau & Hanjalić (2002). The first two of these are fairly widely used and well validated models, thus serving as a reference against which to judge the performance of the more recent BL- $\bar{v}^2/k$  and EBRSM schemes.

The BL- $\bar{v}^2/k$  and the EBRSM are, respectively, elliptic-blending adaptations of the  $\bar{v}^2-f$  and the  $R_{ij}-f_{ij}$  models of Durbin (1991) and Durbin (1993). Both models are designed to take at least some account of the correct near-wall asymptotic behaviour of the Reynolds stresses, without using traditional wall-reflection or other geometry-dependent terms, to simplify application to complex geometries. In both models, a non-dimensional parameter  $\alpha$  is solved for using an elliptic equation of the form:

$$L^2 \partial_{kk} \alpha - \alpha = -1 \quad (1)$$

where  $L$  represents some turbulent length-scale.  $\alpha$  varies from zero at walls to unity in free-stream regions and is used as a blending parameter in both closures.

**The EBRSM formulation:** The parameter  $\alpha$  is here used in the Reynolds stress transport equations to model the pressure strain term,  $\phi_{ij}^*$ <sup>1</sup>, and the dissipation rate,  $\epsilon_{ij}$ , blending between forms devised for the near-wall (subscript  $w$ ) and outer flow (subscript  $h$ ) regions:

---

<sup>1</sup>The term  $\phi_{ij}^*$  in fact represents the sum of the deviatoric pressure-strain,  $\phi_{ij}$ , and the pressure diffusion component.

$$\begin{aligned}\phi_{ij}^* &= (1 - \alpha^3)\phi_{ij,w}^* + \alpha^3\phi_{ij,h}^* \\ \varepsilon_{ij} &= (1 - \alpha^3)\varepsilon_{ij,w} + \alpha^3\varepsilon_{ij,h}\end{aligned}\quad (2)$$

$\varepsilon_{ij,h}$  is simply taken as isotropic,  $2/3\varepsilon\delta_{ij}$ , while the term  $\phi_{ij,h}^*$  is based on the SSG model. In the near-wall region, the model of Rotta (1951) is used for the dissipation rate,  $\varepsilon_{ij,w} = \varepsilon\overline{u_i u_j}/k$ , whilst  $\phi_{ij,w}^*$  is constructed to balance other leading order terms at walls (namely  $\varepsilon_{ij,w}$  and molecular diffusion), and is taken as

$$\phi_{ij,w}^* = -5\frac{\varepsilon}{k}(\overline{u_i u_k n_j n_k} + \overline{u_j u_k n_i n_k} - \frac{1}{2}\overline{u_k u_l n_k n_l}(n_i n_j + \delta_{ij}))\quad (3)$$

where  $\underline{n} = \nabla\alpha$  is used to identify the direction normal to the wall (See Manceau & Hanjalić, 2002, for details).

**The  $\text{BL-}\overline{v^2}/k$  model:** The aim of the more simple elliptic blending eddy viscosity model is to embed in a robust formulation some features of more complex approaches. It uses the blending formulations of equation (2) in a modelled transport equation for the variable  $\varphi = \overline{v^2}/k$ , in addition to a modified  $k$ - $\varepsilon$  system:

$$\frac{Dk}{Dt} = P - \varepsilon - C_{\varepsilon 3}(1 - \alpha)^3 \frac{k}{\varepsilon} E + \partial_j \left( \frac{\nu}{2} + \frac{\nu_t}{\sigma_k} \right) \partial_j k \quad (4)$$

$$\frac{D\varepsilon}{Dt} = \frac{C_{\varepsilon 1}P - C_{\varepsilon 2}^*\varepsilon}{T} + \partial_j \left( \frac{\nu}{2} + \frac{\nu_t}{\sigma_\varepsilon} \right) \partial_j \varepsilon \quad (5)$$

In the  $k$  equation, the inclusion of the term  $E = 2\nu\nu_t(\partial_k j U_i)(\partial_k j U_i)$  (introduced by Jones & Launder (1972) to the  $\varepsilon$  equation), and the factor of two in the denominator of the molecular diffusion, implies that the quantity  $\varepsilon$  has a different definition to that conventionally employed in  $k$ - $\varepsilon$  schemes (*i.e.* a change of variable  $\varepsilon \rightarrow \varepsilon + (1 - \alpha)^3 \frac{k}{\varepsilon} E + \frac{1}{2}\nu\partial_j j k$ ). The coefficient  $C_{\varepsilon 2}^*$  is taken as a function of the turbulent transport of  $k$  to  $\varepsilon$  ratio,  $C_{\varepsilon 2}^* = C_{\varepsilon 2} + \alpha^3(C_{\varepsilon 4} - C_{\varepsilon 2})\tanh\left(\left|\frac{Dk}{\varepsilon}\right|\right)$ , as proposed by Parneix and Laurence (1997). Full details of the scheme can be found in Billard & Laurence (2011) and Billard (2011).

All the models have been implemented in the open source *Code\_Saturne* (Archambeau *et al.*, 2004; Fournier *et al.*, 2011) which is used in the present study. All but the RSM-SSG model are low Reynolds number models which can be integrated all the way to walls. Calculations using the RSM-SSG model use the scalable wall function method of Grotjans & Menter (1998) to handle the near-wall region.

Figure 1 compares the normal Reynolds stresses predicted by the models in the case of plane channel flow for two friction velocity based Reynolds numbers  $Re_\tau = 395$  and  $Re_\tau = 2000$  (DNS data of Kim *et al.* (1987) and Jimenez & Hoyas (2008) are also shown for comparison). The peak and the near-wall behaviour of the Reynolds stresses are well predicted by the EBRSM model. The same conclusion holds for the  $\text{BL-}\overline{v^2}/k$  model as far as the wall normal stress is concerned. As expected, the mean velocity predictions of all models are in good agreement with DNS, and are thus not shown here.

## TWO DIMENSIONAL SEPARATED FLOWS

We now consider the performances of these models in three 2-D flows. The first case considered is the flow over

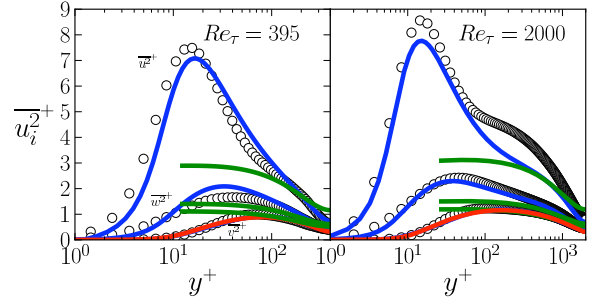


Figure 1. Profiles of the mean Reynolds stresses in a plane channel flow for  $Re_\tau = 395$  and  $Re_\tau = 2000$ ,  $\circ$ DNS —  $\text{BL-}\overline{v^2}/k$ , — SSG, — EBRSM.

periodic 2-D hills, reported by Almeida *et al.* (1992) (reference data taken from the LES of Temmerman and Leschziner (2001)). This is a pressure-induced recirculating flow which has been used quite extensively for comparing the performance of many RANS models (Jang *et al.*, 2002; Temmerman *et al.*, 2003). The geometry is shown in Figure 2 (left): the hill height  $h_1$ , domain height  $H_1$  and inter-hill distance  $L_1$  are such that  $H_1 = 3.036h_1$  and  $L_1 = 9h_1$ , and the Reynolds number, based on the bulk velocity and  $h_1$ , is 10590. The LES study of Fröhlich *et al.* (2005) suggested that this flow features a strong intermittency in the recirculation zone; the modelling of which is out of the reach of RANS models on 2-D grids. Despite this, several simple models are known to return fairly good predictions of the recirculation length, by virtue perhaps of the consideration of such flows during model development.

In the present results, the skin friction coefficient along the bottom wall (Figure 3, left) indicates an over-prediction of the recirculation length by the EBRSM and the  $k$ - $\omega$  SST model, unlike the  $\text{BL-}\overline{v^2}/k$  model which appears to predict a flow pattern closer to that observed in the LES data. This is reflected by the mean stream-wise velocity profiles, shown in figure 4 (top), where it is also seen that the two stress transport models are the most capable of predicting the flow acceleration and resulting near-wall peak of the velocity at the location  $x/h_1 = 0$ .

The turbulent shear-stress predicted across the recirculation bubble at  $x/h_1 = 2$  (Figure 4 (bottom)) is excessively low for all models. This results in a lower level of turbulent mixing between bulk and recirculating flow regions, which explains the over-prediction of recirculation length by the SST and EBRSM schemes. The  $\text{BL-}\overline{v^2}/k$  model performs well in this case, with an accurate prediction of recirculation length, though examination of skin friction coefficient indicates a slight over-prediction of the velocity gradient.

The second case considered is the flow over a wall-mounted hump, reported by Greenblatt *et al.* (2004). The geometry is shown in Figure 2 (centre). The hump chord length  $c$ , its height  $h_2$  and domain height  $H_2$  are related by  $H_2 = 0.91c$  and  $h_2 = 0.128c$ , and the Reynolds number based on  $c$  is  $9.36 \times 10^5$ . In this case the flow separation is induced by the geometry. As an illustration of results, the predicted skin friction coefficient is presented in Figure 3 (centre). All models provide a fair representation of the acceleration over the hump, although the SST scheme underpredicts  $C_f$  here.

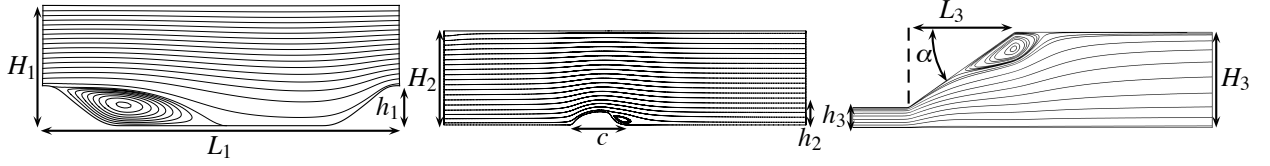


Figure 2. Geometries of the periodic hill (left), the hump (centre) and the diffuser (right) with flow streamlines.

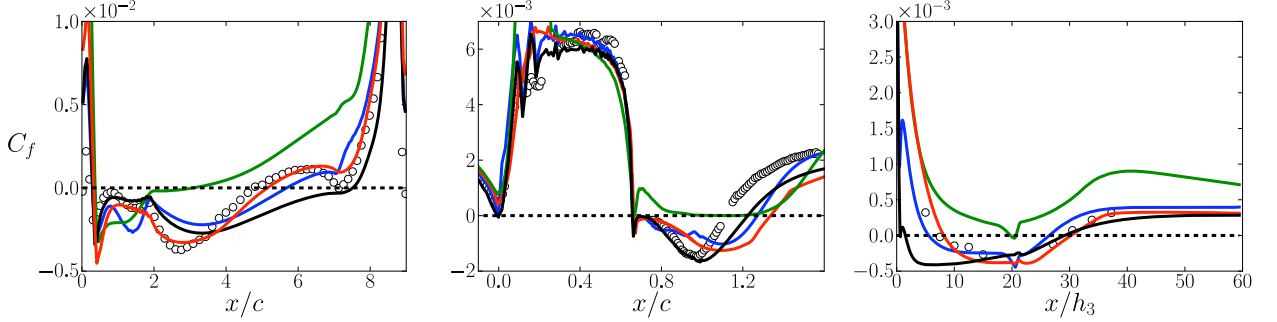


Figure 3. Skin friction coefficient for: the periodic hill (left), the hump (centre) and the 2 dimensional diffuser (right),  $\circ$ Ref. —  $BL-v^2/k$ , —  $k-\omega$  SST, — SSG, — EBRSM.

Conversely, the SST appears to provide a good prediction of the magnitude of the recirculating flow and the closest estimate of the reattachment location, although the recirculation length is overpredicted by all models. The two elliptic-blending based models give good results over the hump, but then over-predict the recirculation length.

The third flow considered is the asymmetric plane diffuser, reported by Buice & Eaton (1997) and Obi *et al.* (1993) (reference data of Obi *et al.* (1993)), pictured in Figure 2 (right). The inlet height  $h_3$ , outlet height  $H_3$  and length of the expanding section  $L_3$  are related by  $H_3 = 4.7h_3$  and  $L_3 = 21h_3$ . The slant angle is  $\alpha = 10^\circ$ , and the Reynolds number based on bulk velocity and  $h_3$  is 18000. The skin friction coefficient along the inclined wall is shown in Figure 3 (right). In this flow, the two elliptic blending based models correctly predict the separation location, compared to a very early separation from the SST and almost no flow reversal when using the SSG (with scalable wall functions). The flow reattachment is better predicted with all schemes, although the EBRSM indicates a somewhat early reattachment.

The rather ambiguous picture provided by these results will perhaps seem familiar to some readers (*i.e.* the more physical RSM's being apparently unable to consistently provide a gain in accuracy). This is quite likely to be linked to the fact that many EVM based schemes are calibrated to 2-D flows such as those considered here, in which a single shear dominates the flow, while the more complex RSM's may perform more consistently over a wider range of complex 2- and 3-D flows.

In view of commonly held opinion that a single “omnipotent” turbulence model is unlikely to emerge, it is useful to re-iterate the importance of model selection. In the following section, we explore the application of the same models to two 3-D separated flows.

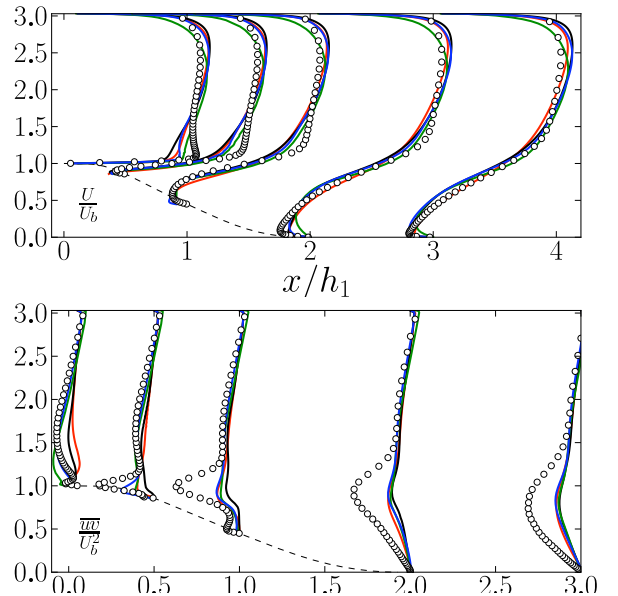


Figure 4. Profiles of mean velocity (top) and turbulent shear stress (bottom) on down-side of periodic hill,  $\circ$ LES —  $BL-v^2/k$ , —  $k-\omega$  SST, — SSG, — EBRSM.

### THREE DIMENSIONAL FLOWS

The case provided in Cherry *et al.* (2008) consists of flow through a three dimensional diffuser (a duct with two contiguous diverging walls), represented in figure 5, with Reynolds number based on bulk velocity and inlet duct height of  $10^4$ . The authors took measurements using Magnetic Resonance Velocimetry, and reported a separation starting at the upper right diverging corner which extended further downstream along the top wall. Only those models capable of resolving anisotropy are able to capture the secondary vortices present

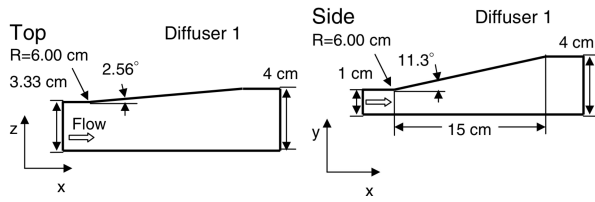


Figure 5. Geometry of the 3D diffuser case.

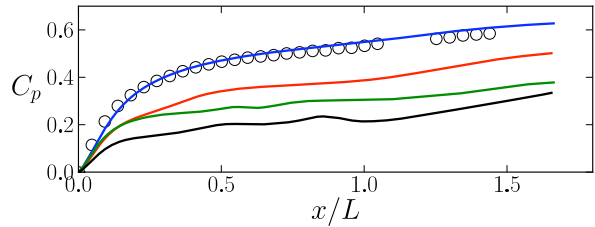


Figure 6. Pressure coefficient along a mid-span line of the lower wall in the 3D diffuser case,  $\circ$ Exp. —  $BL-\overline{v^2}/k$ , —  $k-\omega$  SST, — SSG, — EBRSM.

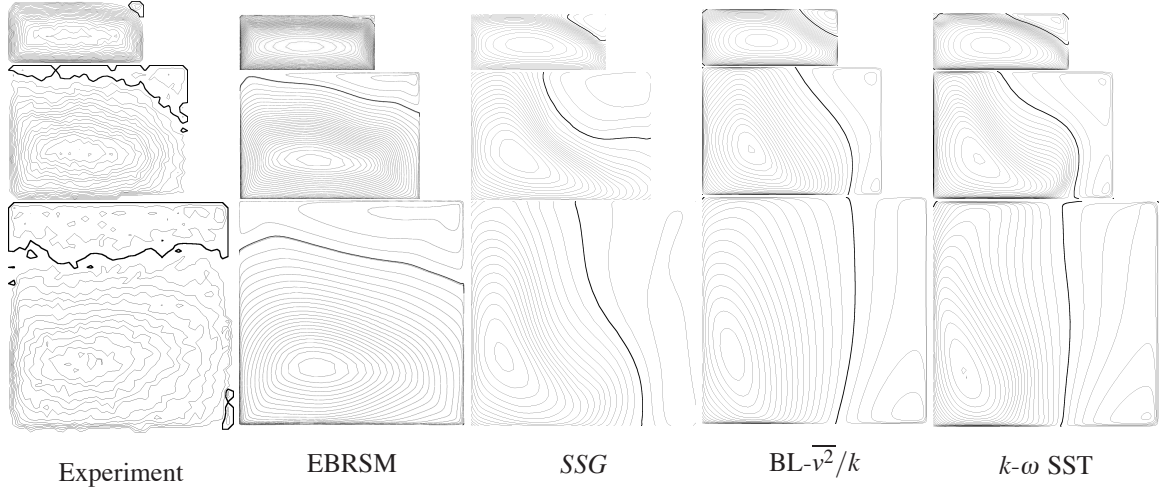


Figure 7. Contours of mean streamwise velocity at three different  $YZ$  planes ( top-bottom,  $x = 2cm$ ,  $x = 8cm$  and  $x = 15cm$  ).

in the inlet and outlet ducts, though at a recent turbulence modelling workshop (Brenn *et al.*, 2008) it was concluded that many RSM's (and most EVMs) predicted the flow recirculation to appear erroneously on the side wall rather than on the top wall.

The simulations were performed on grids of up to  $212 \times 60 \times 180$  points, to obtain grid-independent results, with suitable near-wall refinement to ensure that the nondimensional wall-distance of the near-wall nodes was less than unity. Inflow conditions were taken from precursor periodic duct simulations at the same Reynolds number. Figure 6 presents the evolution of the pressure coefficient,  $C_p$ , along the bottom wall (at midspan), whilst Figure 7 compares the present results with the experimental data in the form of contours of the mean streamwise velocity at four different cross sections (distance  $x$  is defined from the start of the expansion, and the thick line represents the isovalue  $U = 0$ ). As seen from the contours, the EBRSM results are very similar to the experimental data, with the correct location and extent of the recirculation bubble, as confirmed by the  $C_p$  prediction. The SSG returns a corner recirculation which is larger than the experiment at  $x = 2cm$  and which then develops further downstream along the side wall at the end of the diverging section. Its under-prediction of  $C_p$  also reveals a larger flow recirculation than in the experiment. The same erroneous trend is observed for the two EVM's, but the development of the recirculation along the side wall starts earlier ( $x \leq 8cm$ ). Both models also over-predict the recirculation, with particularly poor behaviour returned by the  $k-\omega$  SST model.

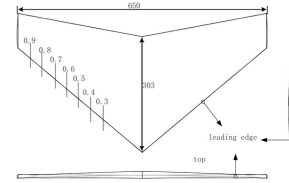


Figure 8. Geometry of the swept wing case.

The difference between EBRSM and SSG results reveals the importance of an accurate near-wall turbulence representation, as this is the major difference between these two models. As linear EVM's, both  $BL-\overline{v^2}/k$  and  $k-\omega$  SST do not capture the secondary flow in the inlet duct. However, this is not the origin of the subsequent discrepancies, since simulations (not shown here) with both models using an inlet field as predicted by the EBRSM scheme also failed to capture the correct separation pattern.

The final case reported here is that of flow separation from a highly swept wing. The 3-D geometry, shown in Figure 8, is a  $40^\circ$  swept wing, at  $9^\circ$  angle of incidence, representing the onset of stall. The Reynolds number based on freestream velocity and root chord length is 210000, and detailed measurement data have been obtained by Zhong & Turner (2007), highlighting a complex flow pattern over the wing. The case was also the object of an Implicit LES reported in Hahn & Drikakis (2009) and a Hybrid RANS/LES simulation of Li & Leschziner (2007).

The computational domain represents half of the wing



Figure 9. Visualisation of instantaneous vorticity (left) and time averaged streamlines (right) of the Implicit LES simulation of Hahn & Drikakis (2009).

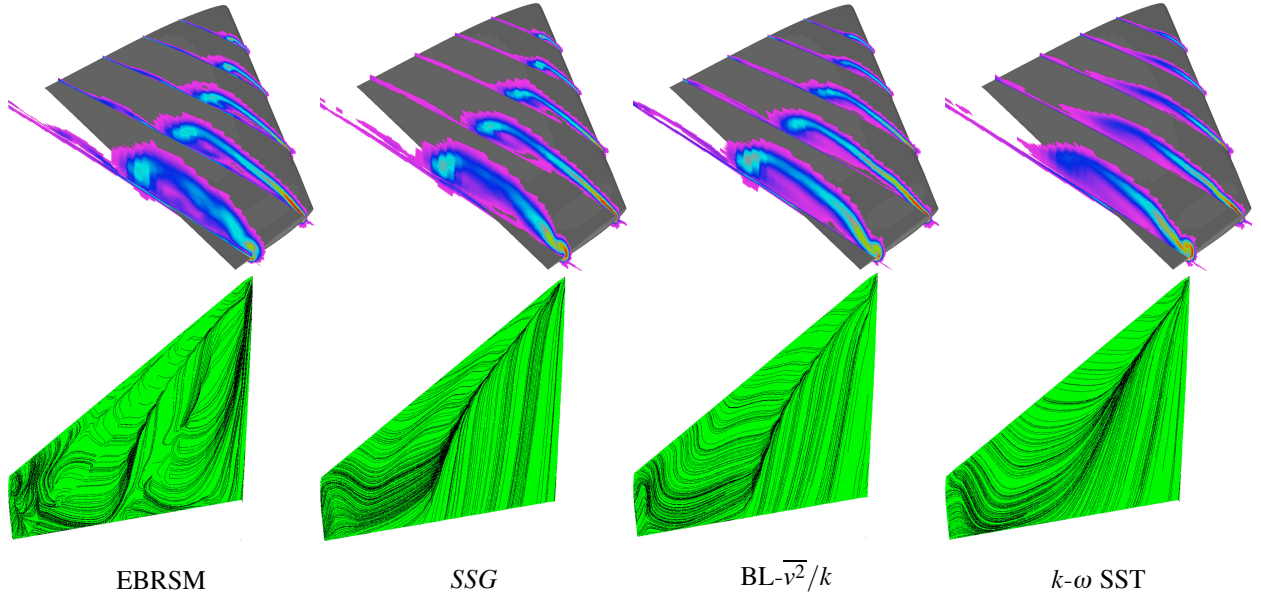


Figure 10. Vorticity contours at different streamwise locations (top) and streamlines (btm) over the wing.

geometry and was meshed with  $256 \times 134 \times 112$  cells (total  $3.8M$ ), using an hyperbolic tangent based refinement in the near-wall region to ensure the presence of enough points within the viscous sublayer; the largest non-dimensional wall-distance of the near-wall nodes was found to be of order 0.5 near the wing tip. Symmetry conditions are prescribed for all variables at the symmetry plane, and freestream inlet turbulence is prescribed so that the associated turbulent lengthscale  $k^{3/2}/\varepsilon$  represents 20% of the chord length. As a consequence of this fully turbulent approach flow, a by-pass transition occurs on the wing.

Figure 10 shows the predicted vorticity on plane cuts over the wing and the streamlines just over the wing. Figure 9 provides equivalent flow visualisations of the implicit LES as presented in Hahn & Drikakis (2009). The leading edge vortex (LEV) captured by all models is comparable to that reported by the LES and experimental data, and is characterized by strong vorticity (as seen in Figure 10) and delimited by the re-attachment line clearly shown by the streamlines. Both the LES and experimental data also report the presence of a secondary vortical region, represented by additional saddles on the surface streamlines within the LEV (as seen on Figure 9, right). This feature is only captured clearly by the EBRSM in the present study, and is also visible in the vorticity plots, where the EBRSM is the only model whose results exhibit a second smaller region of high vorticity beneath the main one. Towards the wing tip the interaction between the LEV and the

opposing outer flow is characterized by another saddle point (see Figure 9, right). Although this is picked up qualitatively by all models, as seen in the streamlines, it is best represented by the two elliptic blending based models.

Hahn & Drikakis (2009) also reported a further flow feature inboard of the main vortex, where their simulation predicted a portion of fluid revolving around a focal point and a separation zone near the trailing edge. In contrast, the experimental data only showed streamlines aligned with the freestream direction here. It is interesting to note that the EBRSM results indicate a similar feature, whereas the SSG and both EVM's show trends similar to that of the experiment.

Mean stream-wise velocity predictions are compared to Laser Doppler Anemometry (LDA) experimental profiles in Figure 11 at 50% span (as indicated on Figure 8), for 5 different chord-wise locations. At this location the secondary vorticity is captured by the EBRSM from the first station (10% chord) where the profiles are marked by a wiggle visible at 10%, 30% and 50% chord. It can also be seen in the experiment at the same locations but with a smaller amplitude (though a change in the profile concavity is still clearly visible). This secondary vortical region also appears on the SSG profiles, but somewhat displaced (at 30% chord). Although this feature is totally missed by the  $k-\omega$  SST model (which predicts monotonic profiles until the peak) the  $BL-\overline{v^2}/k$  model also captures a near-wall velocity kink but at considerably greater chord lo-

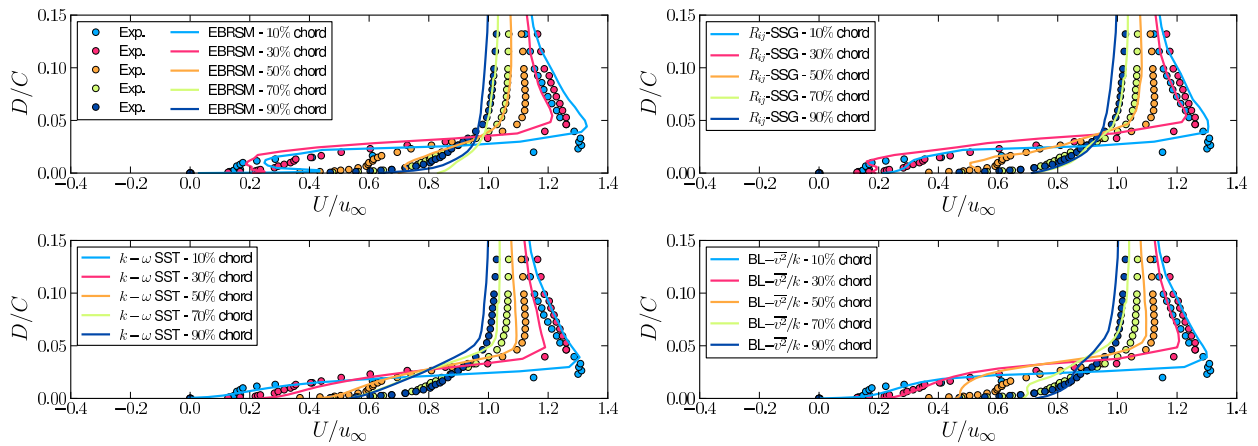


Figure 11. Velocity profiles at different chord location at 50% span over the wing.

cation (50% chord). The location of the velocity peak for all four models is displaced away from the wall at 10% and 30% chord locations, suggesting an excessive size of the LEV.

Approaching the wing tip (80% span), velocity profiles (not shown here) reveal that the experimental data exhibits a near-wall region of negative stream-wise velocity over all the chord length, which is only partially captured by the models (both elliptic relaxation based models only predict a negative velocity for the two first chord locations). All models except the  $k-\omega$  SST under-predict the magnitude of the velocity peak, but conversely the latter model under-predicts the boundary layer thickness across the wing chord.

## CONCLUSION

Differences between eddy viscosity modelling and second moment closure, as well as the effects of the near-wall turbulence representation, are illustrated by the variability of results obtained in the five cases considered. While no clear conclusions are drawn from the 2-D cases alone, some of the flow features (such as the marked acceleration on the uphill side of the periodic hill, or the secondary vorticity appearing on the swept wing) are captured only with the most advanced model considered, the EBRSM. This is also the only model able to predict the correct development of the recirculation in the 3-D diffuser flow. These observations support the principle that flows with strong 3-D effects, involving multiple-shears as opposed to a single shear, necessitate stress anisotropy resolution. The importance of near wall modelling is also highlighted by observing the results of the SSG model in high Reynolds form. These results justify the careful selection of the underlying RANS model in a hybrid RANS-LES approach, as some of the modelling improvements considered here (in particular in the near-wall region) would be active where such approaches are in RANS mode.

**Acknowledgements:** The authors gratefully acknowledge computational support from EPSRC for UKs National HPC Facility, HEC-ToR, via Direct Access Class 1b. This work was supported in part by the EC project ATAAC, 7th Framework Prog. (No. ACP8-GA-2009-233710-ATAAC). The authors are also grateful to N. Li and M. Leschziner for providing the mesh for the Swept Wing case.

## REFERENCES

- Almeida, G.P., Durao, D.F.G. & Heitor, M.V. 1992 *Exp. Thermal and Fluid Science* p. 87.
- Archambeau, F., Mechtoua, N. & Sakiz, M. 2004 *International Journal on Finite Volumes* 1 (1).
- Billard, F. 2011 PhD thesis, School of Mechanical Aerospace and Civil Engineering - The University of Manchester, to appear.
- Billard, F & Laurence, D 2011 *Submitted to International Journal of Heat and Fluid Flow*.
- Brenn, G., Jakirlic, S. & Steiner, H. editors. 2008 *13<sup>th</sup> SIG15 ERCOFTAC Workshop on Refined Turbulence Modelling*, Graz, Austria
- Buice, CU & Eaton, JK 1997 Report TSD-107, Department of mechanical engineering.
- Cherry, E.M., Elkins, C.J. & Eaton, J.K. 2008 *International Journal of Heat and Fluid Flow* 29 (3), 803–811.
- Durbin, P.A. 1991 *Theoretical and Computational Fluid Dynamics* 3 (1), 1–13.
- Durbin, P.A. 1993 *Journal of Fluid Mechanics* 249, 465–498.
- Fournier, Y., Bonelle, J., Moulinec, C., Shang, Z., Sunderland, AG & Uribe, JC 2011 *Computers & Fluids* 45 (1), 103–108.
- Fröhlich, J., Mellen, C.P., Rodi, W., Temmerman, L. & Leschziner, M.A. 2005 *Journal of Fluid Mechanics* 526, 19–66.
- Fröhlich, J. & von Terzi, D. 2008 *Progress in Aerospace Sciences* 44 (5), 349–377.
- Greenblatt, D., Paschal, K.B., Yao, C.S., Harris, J., Schaeffler, N.W. & Washburn, A.E. 2004 *AIAA Paper* 2220, 2004.
- Grotjans, H. & Menter, F. 1998. In *Proceedings of the 4th European Computational Fluid Dynamics Conference*, John Wiley & Sons, pp. 1112–1117.
- Haase, W., Auipoix, B., Bunge, U. & Schwamborn, D., 2006. Notes on Numerical Fluid Mechanics and Multidisciplinary Design. Vol. 94. Springer, Heidelberg.
- Haase, W., Braza, M. & Revell, A. 2009 Notes on Numerical Fluid Mechanics and Multidisciplinary Design, Vol. 103.
- Hahn, M. & Drikakis, D. 2009 *AIAA journal* 47 (3), 618–630.
- Jang, YJ, Leschziner, MA, Abe, K. & Temmerman, L. 2002 *Flow, Turbulence and Combustion* 69 (2), 161–203.
- Jimenez, Javier & Hoyas, S. 2008 *Journal of Fluid Mechanics* 611, 215–236.
- Jones, WP & Launder, B. 1972 *International Journal of Heat and Mass Transfer* 15 (2), 301–314.
- Kim, J., Moin, P. & Moser, R. 1987 *Journal of Fluid Mechanics* 177, 133–166.
- Li, N. & Leschziner, MA 2007 *Aeronautical Journal* 111 (1125), 689–698.
- Manceau, R. & Hanjalić, K. 2002 *Physics of Fluids* 14 (2), 744–754.
- Menter, F.R. 1994 *AIAA journal* 32 (8), 1598–1605.
- Obi, S., Aoki, K. & Masuda, S. 1993 *Proceedings 9th Symp. of Turbulent Shear Flow*, Kyoto, Japan.
- Rotta, J. 1951 *Zeitschrift für Physik A Hadrons and Nuclei* 129 (6), 547–572.
- Speziale, C.G., Sarkar, S. & Gatski, T.B. 1991 *Journal of Fluid Mechanics* 227 (-1), 245–272.
- Sveningsson, A., Pettersson-Reif, B.A. & Davidson, L. 2005 In *Proceedings of the 4<sup>th</sup> International Symposium on Turbulence and Shear Flow Phenomena*, Williamsburg, VA, USA.
- Temmerman, L., Leschziner, M., 2001 In: *Int. Symp. Turb. Shear Flow Phenomena*, Stockholm, Sweden.
- Temmerman, L., Leschziner, M.A., Mellen, C.P. & Fröhlich, J. 2003 *International Journal of Heat and Fluid Flow* 24 (2), 157–180.
- Zhong, S. & Turner, J, MSTTAR Project, EPSRC GR/S27443/01.